

# Diffusion Changes in Hippocampal Cingulum in Early Biologically Defined Alzheimer's Disease

Qianyun Chen, Jill Abrigo, Min Deng, Lin Shi, Yi-Xiang Wang, Winnie Chiu Wing Chu\* and for the Alzheimer's Disease Neuroimaging Initiative<sup>1</sup>  
*Department of Imaging and Interventional Radiology, Faculty of Medicine, The Chinese University of Hong Kong, Hong Kong SAR, China*

Accepted 23 November 2022  
Pre-press 14 December 2022

## Abstract.

**Background:** Diagnosis of Alzheimer's disease (AD) was recently shifted from clinical to biological construct to reflect underlying neuropathological status, where amyloid deposition designated patients to the Alzheimer's continuum, and additional tau positivity represented AD.

**Objective:** To investigate white matter (WM) alteration in the brain of patients in the Alzheimer's continuum.

**Methods:** A total of 236 subjects across the clinical and biological spectra of AD were included and stratified by normal/abnormal (–/+) amyloid (A) and tau (T) status based on positron emission tomography results, yielding five groups: A–T– cognitively normal (CN), A+T– CN, A+T+ CN, A+T+ mild cognitive impairment, and A+T+ AD. WM alteration was measured by diffusion tensor imaging (DTI). Group differences, correlation of DTI measures with amyloid and tau, and diagnostic performance of such measures were evaluated.

**Results:** Compared with A–T– CN, widespread WM alteration was observed in the Alzheimer's continuum, including hippocampal cingulum (CGH), cingulum of the cingulate gyrus, and uncinate fasciculus. Diffusion changes measured by regional mean fractional anisotropy (FA) in the bilateral CGH were first detected in the A+T+ CN group and associated with tau burden in the Alzheimer's continuum ( $p < 0.001$ ). For discrimination between A+T+ CN and A–T– CN groups, CGH FA achieved accuracy, sensitivity, and specificity of 74%, 58%, and 78% for right CGH and 57%, 83%, and 47% respectively for left CGH.

**Conclusion:** WM alteration is widespread in the Alzheimer's continuum. Diffusion alteration in CGH occurred early and was correlated with tau pathology, thus may be a promising biomarker in preclinical AD.

Keywords: Alzheimer's disease, amyloid- $\beta$ , diffusion tensor imaging, hippocampal cingulum, tau

## INTRODUCTION

Alzheimer's disease (AD) is characterized by two hallmarks, namely, amyloid- $\beta$  ( $A\beta$ ) and neurofibrillary tangles composed of phosphorylated tau, which occurs for years prior to the presentation of clinical symptoms. Detecting AD-related pathological changes during the asymptomatic stage is important not only to understand disease mechanisms and progression but also to allow potential intervention and facilitate recruitment in clinical trials [1]. Currently,  $A\beta$  and tau can only be confirmed on postmortem examination [2], which has driven research impetus for the identification of *in vivo* imaging biomarkers

<sup>1</sup>Data used in preparation of this article were obtained from the Alzheimer's Disease Neuroimaging Initiative (ADNI) database (adni.loni.usc.edu). As such, the investigators within the ADNI contributed to the design and implementation of ADNI and/or provided data but did not participate in analysis or writing of this report. A complete listing of ADNI investigators can be found at: [http://adni.loni.usc.edu/wp-content/uploads/how\\_to\\_apply/ADNI\\_Acknowledgement\\_List.pdf](http://adni.loni.usc.edu/wp-content/uploads/how_to_apply/ADNI_Acknowledgement_List.pdf)

\*Correspondence to: Professor Winnie Chiu Wing Chu, Room 27026, G/F, Treatment Block & Children Wards, Department of Imaging & Interventional Radiology, Prince of Wales Hospital, Shatin, Hong Kong SAR, China. Tel.: +86 852 35052299; E-mail: winniechu@cuhk.edu.hk.

to aid in AD diagnosis. Measures for *in vivo* A $\beta$  and tau detection include positron emission tomography (PET) and cerebrospinal fluid (CSF) via lumbar puncture. However, the widespread use of these methods is hindered because of the limited availability of radioactive tracers, expensive cost, and inherent invasiveness. Structural brain imaging may show hippocampal volume loss, but this occurs in the late stage of the disease and is not specific to AD, as it can also be age-related and present in non-AD forms of dementia [3].

White matter (WM) abnormalities are also commonly present among patients with AD and may be a sign of an early neuropathologic event [4]. Diffusion tensor imaging (DTI) studies revealed WM demyelination and axonal loss in mild cognitive impairment (MCI) and preclinical AD [5]. DTI is an MRI technique that quantifies the magnitude and directionality of the molecular diffusion of water along axonal tracts, allowing the assessment of WM integrity [6]. Diffusion in normal axons tends to be limited and parallel to tracts, whereas diffusion in damaged WM exhibits lower fractional anisotropy (FA) and higher mean diffusivity (MD). Results from DTI studies show that altered WM tracts are widespread at the stages of MCI and AD [7] in specific regions related to cognitive decline [8], and in the hippocampal cingulum, corpus callosum, and fornix [8–10]. Changes in WM have also been reported to precede symptom onset [11], and may be linked to deposition of A $\beta$  [12, 13] and tau [6, 14, 15], suggesting their early involvement in the course of AD. These findings lend support to the notion that WM changes measured by DTI could provide useful information for clinical diagnosis of patients with AD.

Approximately 10% to 30% of clinically diagnosed AD dementia do not display AD pathologic change at autopsy [16], while 30% to 40% of cognitively unimpaired elderly persons have AD pathology at autopsy [17]. To better reflect underpinning neuropathology, the diagnosis of AD has been shifted from clinical to biological in the research setting. Only individuals with abnormal A $\beta$  deposits are considered to be in the Alzheimer's continuum, which is further divided into two phases: Alzheimer's pathologic change [individuals with abnormal A $\beta$  but normal tau biomarker (A+T-)] and AD [individuals with abnormal A $\beta$  and tau biomarkers (A+T+)] [18]. It remains unclear how WM changes in the Alzheimer's continuum with A $\beta$ , tau, and cognitive status considered. The main objective of the present study was to determine the patterns of WM alterations

on DTI in subjects within the Alzheimer's continuum at different clinical stages. The second objective was to explore the association of WM microstructural changes with A $\beta$  and tau burden within the Alzheimer's continuum. The third objective was to explore the diagnostic performance of regional mean FA values derived from DTI in the preclinical stage of AD defined by the biological markers.

## MATERIALS AND METHODS

### *Subjects*

All data was acquired from the Alzheimer's Disease Neuroimaging Initiative 3 database (ADNI 3) (<http://adni.loni.usc.edu/>). The ADNI was launched in 2003 as a public-private partnership, led by Principal Investigator Michael W. Weiner, MD. The primary goal of ADNI has been to test whether serial MRI, PET, other biological markers, and clinical and neuropsychological assessments can be combined to assess the progression of MCI and early AD. ADNI includes men and women aged 55–90 years across cognitively normal (CN), MCI, and AD dementia groups. The clinical diagnosis was given according to the criteria of the National Institute of Neurological and Communicative Disorders and Stroke-Alzheimer's Disease and Related Disorders Association (NINCDS-ADRAD) [19].

For the current study, participants at various clinical stages who underwent T1-weighted MRI, DTI, AV45 Flortbetapir PET, and AV1451 Flortaucipir PET at ADNI3 baseline were included. Demographic information such as age, sex, years of education, Clinical Dementia Rating (CDR), Mini-Mental State Exam (MMSE), and clinical diagnosis were recorded.

### *Biomarker group classification and PET analysis*

According to the National Institute on Aging and Alzheimer's Association (NIA-AA) 2018 research framework [18], A $\beta$  determines if individuals have Alzheimer's pathologic change (A+T-), and both A $\beta$  and pathologic tau are required for a diagnosis of AD (A+T+). In this study, we followed the NIA-AA recommendations and selected subjects mainly by A and T biomarker profiles. Clinical diagnosis was used for staging severity. In addition, we hypothesized that white matter diffusion change occurs at an early stage, therefore subjects were categorized into the following groups: 1) CN subjects with normal A $\beta$  and tau (A-T- CN); 2) CN subjects with abnormal A $\beta$  but

normal tau (A+T–CN); 3) CN subjects with abnormal A $\beta$  and tau (A+T+ CN); 4) MCI with abnormal A $\beta$  and tau (A+T+ MCI); and 5) dementia with abnormal A $\beta$  and tau (A+T+ AD).

A $\beta$  and tau status were determined using AV45 florbetapir and AV1451 flortaucipir PET values provided by the University of California, Berkeley. The AV45 florbetapir PET was used to assess global A $\beta$  load. The mean standard uptake value ratio (SUVR) on AV45 PET was calculated from the cortical summary regions-of-interest (ROIs), including frontal, anterior/posterior cingulate, lateral parietal, and lateral temporal regions, with whole cerebellum as reference region. A cut-off value of 1.11 was applied to determine A $\beta$  positivity (A+) [20]. The AV1451 Flortaucipir PET SUVR values were used to quantify tau burden in the AD signature regions. Briefly, a size-weighted mean Flortaucipir SVUR was calculated in temporal meta-ROI including amygdala, entorhinal, fusiform, inferior temporal and middle temporal gyri, and normalized by inferior cerebellar gray matter. Tau positivity (T+) was thresholded at an SUVR of >1.23 [21].

#### Structural MRI acquisition and analysis

Image protocols were standardized across ADNI study sites. 3D T1-weighted volumetric sequences were acquired with the following parameters: echo time (TE)=2.98 ms, repetition time (TR)=2300 ms, inversion time=900ms, flip angle=10°, field of view (FOV)=208 × 240 × 256 mm<sup>3</sup>, acquired resolution=1 × 1 × 1 mm<sup>3</sup>. The details of the MRI parameters can be found at <http://adni.loni.usc.edu/methods/documents/mri-protocols/>.

T1-weighted images were corrected for head motion and intensity inhomogeneity, followed by removal of non-brain tissue using the pipeline implemented in Freesurfer version 7.1 (<http://surfer.nmr.mgh.harvard.edu/>). Skull-stripped volumes were visually inspected and manually modified when needed. Hippocampal volume (HV) and estimated total intracranial volume (eTIV) were derived from Freesurfer output. HV was normalized by eTIV using the following formula [14]:

$$\text{Adjusted HV} = \text{raw HV} - b(\text{eTIV} - \text{mean eTIV}) \quad (1)$$

where  $b$  indicates the regression coefficient when HV is regressed against eTIV.

Considering that white matter hyperintensities (WMH) shown on T2 FLAIR images are possible

factors associated with vascular disease and may influence DTI measures on WM [22], we controlled for WMH volumes in the statistical analysis. WMH volumes were obtained from ADNI, which was estimated with a modified Bayesian probability structure based on the method of histogram fitting. Briefly, the likelihood estimates of each image were calculated through histogram segmentation and thresholding. Then, along with WMH priors (which were estimated from more than 700 individuals) and tissue constraints, the probabilities were thresholded at 3.5 standard deviations above the mean to create a binary WMH mask. Finally, the mask was back-transformed to native space for volume calculation. The WMH volumes were available for all included subjects.

#### DTI acquisition and analysis

Six  $b_0$  images and 48 diffusion-weighted DWI scans at  $b$  value=1000 s/mm<sup>2</sup> were acquired at 2 × 2 × 2 mm<sup>3</sup> resolution (GE: time repetition, 7800 ms; flip angle, 90°; time echo, 55–62 ms; field of view, 232 × 232 × 138 mm. Siemens: time repetition, 7200–9600 ms; time echo, 56–82 ms; flip angle, 90°; field of view, 232 × 232 × 160 mm<sup>3</sup>). For each subject, raw DWI volumes were first corrected for head motion and eddy-current distortions with the *eddy\_correct* tool from the FMRIB software library (FSL) (<http://www.fmrib.ox.ac.uk/fsl>).  $b$  vectors were rotated accordingly [23]. All non-brain tissues were removed from diffusion-weighted images using the FSL's Brain Extraction Tool. Skull-stripped  $b_0$  images were registered to their respective corrected T1-weighted scans based on white-matter boundaries using the FSL's *epi\_reg* tool. The resulting 3D transformation matrices and deformation fields were applied to the remaining DWI volumes. Lastly, a single diffusion tensor was fitted at each voxel in the brain by using FSL's DTIFIT program, and the diffusion tensor eigenvalues obtained were used to calculate FA and MD maps. All processed images were visually inspected for quality control. Thirty-five images were excluded from further analysis due to excessive distortion artifacts.

To derive DTI measures from specific WM tracts, the Johns Hopkins University–International Consortium of Brain Mapping (JHU-ICBM)-DTI atlas [24] containing 48 WM tracts was used. The list of tracts in the atlas is presented in the Supplementary Table 1. The DTI atlas was first linearly and then non-linearly registered to each individual's FA maps using FSL's registration tools [25, 26]. The derived deformation

field was then applied on the WM label to obtain WM ROIs in the individual spaces. Voxels with FA value  $<0.2$  were excluded from the ROIs. The WM ROI was superimposed on FA and MD maps separately to extract mean values.

### Statistical analysis

The normality of continuous variables was first examined by Shapiro–Wilk test in which the assumption of normality was violated. WMH was log-transformed for subsequent analysis due to its skewness. Group comparisons for continuous variables with skewed distribution were performed using Kruskal–Wallis test along with Mann–Whitney U test for *post hoc* comparison; otherwise, analysis of variance followed by Scheffe’s tests was conducted for normally distributed variables. Chi-square test was employed to analyze categorical variables.

To evaluate the group difference in diffusion metrics of 48 atlas-based tracts, analysis of covariance (ANCOVA) was performed with control of age, sex, years of education, and WMH volumes. Bonferroni method ( $p < 0.05/48$ ) was used to adjust for false-positive results in multiple comparisons of 48 atlas-based regions of interest. If the ANCOVA results were significant, *post hoc* comparisons were then performed with the Bonferroni method.

To assess the association of DTI measures with global A $\beta$  load and tau burden in the temporal meta-ROI, we formulated a regression model with FA/MD value as dependent variable, while A $\beta$  and tau as well as four covariates (age, sex, years of education, and WMH volume) were used as independent variables. Correlation of DTI measures with HV was also assessed. For these analyses, we verified the normal distribution of the residuals, the absence of heteroscedasticity, and the lack of multicollinearity between the variables, which was determined using a variance inflation factor below 10. A regression model was built in each of the following cohorts: (i) the Alzheimer’s continuum group (all groups except for A–T– CN group), (ii) the A–T– CN group, (iii) the A+T– CN group, and (iv) the A+T+ CN group. The  $p$  value was adjusted for multiple comparisons with the Bonferroni method ( $p < 0.05/4$ ).

To evaluate the diagnostic performance of DTI measures, we analyzed the receiver operating characteristic (ROC) curves. We focused on detecting AD pathology in subjects without presenting clinical symptoms, so we performed the following classification among CN subjects: 1) A–T– CN versus A+T–

CN; 2) A–T– CN versus A+T+ CN; 3) A+T– CN versus A+T+ CN. HV was included for comparison as it is the most established biomarker of AD [3]. Diagnostic performance was evaluated using the area under the ROC curve (AUC). The optimal cutoff for positivity was determined using the Youden Index [27]. Accuracy, sensitivity, and specificity were calculated based on the derived cutoff value. DeLong’s test [28] was performed to compare differences in the performance of various diagnostic metrics. All statistical analyses were performed using SPSS 26.0 (Armonk, NY). Statistical tests were two-sided, with a significance level set to  $p < 0.05$ .

## RESULTS

### Demographics

A total of 236 subjects were included, comprised of 97 A–T– CN, 43 A+T– CN, 36 A+T+ CN, 35 A+T+MCI, and 24 A+T+AD. The demographic details are presented in Table 1. The groups were comparable in terms of sex ( $p = 0.51$ ) but different in terms of years of education ( $p = 0.02$ ), age, CDR, MMSE, WMH volumes, global florbetapir SUVR, flortaucipir SUVR, and hippocampal volume (all with  $p < 0.001$ ).

### Group comparisons

For FA, significant differences across five groups were found in the tracts of fornix, hippocampal cingulum (CGH), cingulum of the cingulate gyrus (CGC), and uncinate fasciculus (UF) after controlling for age, sex, years of education, and WMH volume (fornix,  $F(4, 227) = 6.84$ ,  $p < 0.001$ ; right CGH,  $F(4, 227) = 9.47$ ,  $p < 0.001$ ; left CGH,  $F(4, 227) = 12.38$ ,  $p < 0.001$ ; right CGC,  $F(4, 227) = 5.58$ ,  $p < 0.001$ ; left CGC,  $F(4, 227) = 5.50$ ,  $p < 0.001$ ; right UF,  $F(4, 227) = 5.82$ ,  $p < 0.001$ ; left UF,  $F(4, 227) = 5.50$ ,  $p < 0.001$ ). In general, FA in CN groups was higher than that in MCI and AD groups. Specifically, compared with the A–T– CN group, A+T+ AD group showed lower FA values in the tracts of fornix, CGH, CGC, and UF (all with  $p < 0.001$ ), while the A+T+ MCI group showed lower FA values in the bilateral CGH tract (all with  $p < 0.001$ ). The A+T+ AD and A+T+ MCI groups showed lower FA in the tracts of fornix, CGH, CGC and UF than the A+T– CN group, with  $p < 0.001$  for the A+T+ AD group and  $p < 0.05$  for the A+T+ MCI group. The FA was significantly reduced between A+T+ CN and A+T+ AD

Table 1  
Cohort characteristics

	A-T- CN (a)	A+T- CN (b)	A+T+ CN (c)	A+T+ MCI (d)	A+T+ AD (e)	<i>p</i>
N	97	43	36	36	24	
Sex: F/M (%F)	52/45 (54%)	25/18 (58%)	24/12 (67%)	22/14 (61%)	11/13 (46%)	0.51
Age	71.1 (6.3)	75.3 (8.3)	76.5 (5.9)	74.9 (7.6)	78.6 (9.4)	<0.001 <sup>†</sup>
Education (y)	16 (16–18)	18 (14–18)	17 (15–19)	16 (15–18)	15 (12–16)	0.02 <sup>††</sup>
CDR	0 (0-0)	0 (0-0)	0 (0-0)	1 (1-1)	1 (1-1)	<0.001 <sup>†††</sup>
MMSE	29 (29-30)	29 (28–30)	29 (27–30)	28 (26–29)	22 (17–24)	<0.001 <sup>§</sup>
WMH (cm <sup>3</sup> )	1.1 (0.4–2.6)	2.2 (0.7–10.0)	2.2 (0.9–10.5)	2.6 (0.9–7.8)	3.4 (2.0–7.2)	<0.001 <sup>§§</sup>
Global amyloid SUVR	1.02 (0.98–1.05)	1.17 (1.14–1.30)	1.29 (1.19–1.49)	1.44 (1.29–1.58)	1.44 (1.31–1.61)	<0.001 <sup>§§§</sup>
Tau SUVR	1.16 (1.12–1.19)	1.16 (1.12–1.20)	1.27 (1.25–1.34)	1.41 (1.31–1.65)	1.57 (1.37–2.27)	<0.001 <sup>¶</sup>
Hippocampal volume (cm <sup>3</sup> )	8.1 (0.8)	7.9 (0.8)	7.8 (0.7)	7.2 (0.9)	6.5 (0.9)	<0.001 <sup>¶¶</sup>

Values are expressed as mean with standard deviation for normal distribution data, otherwise expressed as median with interquartile range. CN, cognitively normal; MCI, mild cognitively impairment; AD, Alzheimer's disease; CDR, Clinical Dementia Rating; MMSE, Mini-Mental State Exam; WMH, white matter hyperintensities; SUVR, standard uptake value ratio. <sup>†</sup>Statistically significant difference between (a) versus (c), and between (a) versus (e). <sup>††</sup>Statistically significant difference between (a) versus (e), and between (c) versus (e). <sup>†††</sup>Statistically significant difference between (a) versus (d)(e), and between (b) versus (d)(e), and between (c) versus (d)(e). <sup>§</sup>Statistically significant difference between (a) versus (d)(e), and between (b) versus (d)(e), and between (e) versus (c)(d). <sup>§§</sup>Statistically significant difference between (a) versus (c)(d)(e). <sup>§§§</sup>Statistically significant difference between (a) versus (b)(c)(d)(e), and between (b) versus (d)(e). <sup>¶</sup>Statistically significant difference between (a) versus (c)(d)(e), and between (b) versus (c)(d)(e). <sup>¶¶</sup>Statistically significant difference between (a) versus (d)(e), and between (b) versus (d)(e), and between (c) versus (e).

for the tracts of fornix, CGH, CGC, and UF (all with  $p < 0.01$ ) and between A+T+ MCI and A+T+ AD for the tracts of bilateral CGH, CGC, and UF (all with  $p < 0.05$ ). Among three CN groups, both right and left CGH FA showed a significant difference between A-T- CN and A+T+ CN groups, and left CGH FA presented a significant decrease in A+T+ CN compared with A+T- CN group (Fig. 1).

Regarding MD, significant differences across five groups were found in the tracts of genu of the corpus callosum (GCC), body of the corpus callosum (BCC), splenium of the corpus callosum (SCC), CGC, CGH, superior longitudinal fasciculus (SLF), and UF (all with  $p < 0.001$ ). (GCC,  $F(4, 227) = 7.80$ ,  $p < 0.001$ ; BCC,  $F(4, 227) = 7.96$ ,  $p < 0.001$ ; SCC,  $F(4, 227) = 6.41$ ,  $p < 0.001$ ; right CGC,  $F(4, 227) = 8.06$ ,  $p < 0.001$ ; left CGC,  $F(4, 227) = 7.86$ ,  $p < 0.001$ ; right CGH,  $F(4, 227) = 21.62$ ,  $p < 0.001$ ; left CGH,  $F(4, 227) = 29.48$ ,  $p < 0.001$ ; right SLF,  $F(4, 227) = 5.67$ ,  $p < 0.001$ ; left SLF,  $F(4, 227) = 6.73$ ,  $p < 0.001$ ; right UF,  $F(4, 227) = 8.01$ ,  $p < 0.001$ ; left UF,  $F(4, 227) = 8.81$ ,  $p < 0.001$ ). In general, MD in the MCI and AD groups were higher than that in the CN groups and was comparable among CN groups. Specifically, compared with the A-T- CN group, both A+T+ AD and A+T+ MCI

groups showed higher MD in the tracts of GCC, BCC, SCC, CGC, CGH, SLF, and UF. Compared with the A+T- CN group, the A+T+ AD group showed higher MD in the tracts of GCC, BCC, SCC, CGC, CGH, SLF, and UF (all with  $p < 0.001$ ), while the A+T+ MCI group showed higher MD in these tracts (all with  $p < 0.05$ ) except for left UF ( $p = 0.68$ ). Compared with the A+T+ CN group, the A+T+ AD group showed higher MD in the tracts of GCC, BCC, SCC, CGC, CGH, SLF, and UF (all with  $p < 0.001$ ), while the A+T+ MCI group showed higher MD in the tracts of BCC ( $p = 0.04$ ), GCC ( $p = 0.03$ ), right CGC ( $p = 0.01$ ), bilateral CGH (all with  $p < 0.01$ ), bilateral SLF (all with  $p = 0.02$ ), and right UF ( $p < 0.01$ ). No significant difference was found among the three CN groups.

#### Association of DTI measures in CGH with global $A\beta$ load, tau burden in the temporal meta-ROI, and HV

Bilateral CGH was the only tract that showed FA changes among CN groups, and consistently showed lower FA in the A+T+ CN, A+T+ MCI, and A+T+ AD groups when compared with the A-T- CN group. In this regard, we further investigated

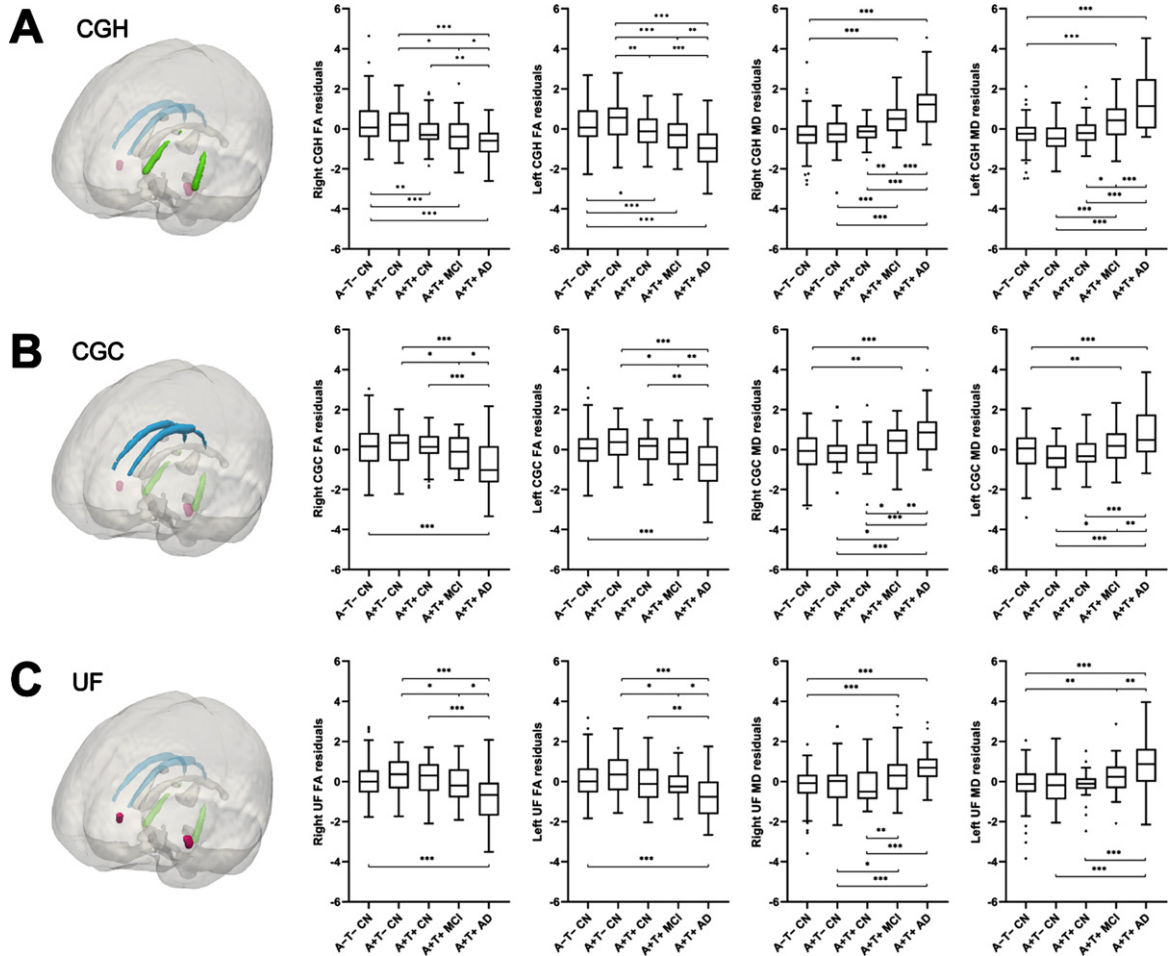


Fig. 1. Comparison of FA (first and second column) and MD (third and fourth column) across groups in the bilateral CGH (A), CGC (B), and UF (C). The boxplots show the median and inter-quartile range. The values presented in the y-axis are the residuals of FA or MD after regressing out the effect of age, sex, years of education and WMH volume with linear regression models. CGH, hippocampal cingulum; CGC, cingulum of cingulate gyrus; UF, uncinate fasciculus; FA, fractional anisotropy; MD, mean diffusivity; CN, cognitively normal; MCI, mild cognitive impairment; AD, Alzheimer's disease. A-/A+, negative/positive amyloid-PET; T-/T+, negative/positive tau-PET. \* $p < 0.05$ ; \*\* $p < 0.01$ ; \*\*\* $p < 0.001$ .

its association with the global A $\beta$ , tau in the temporal meta-ROI, and HV. The results are shown in Table 2 and Fig. 2. For subjects in the Alzheimer's continuum, FA and MD in the bilateral CGH were associated with tau PET SUVR and HV but not with A $\beta$  PET SUVR. Specifically, lower FA was associated with greater tau burden in right CGH ( $\beta = -0.23$ ,  $p < 0.001$ ) and left CGH ( $\beta = -0.29$ ,  $p < 0.001$ ), and higher MD was associated with greater tau burden in right CGH ( $\beta = 0.30$ ,  $p < 0.001$ ) and left CGH ( $\beta = 0.36$ ,  $p < 0.001$ ). Lower FA correlated with lower HV in the right CGH ( $\beta = 0.39$ ,  $p < 0.001$ ) and left CGH ( $\beta = 0.40$ ,  $p < 0.001$ ), and higher MD correlated with lower HV in the right CGH ( $\beta = -0.44$ ,  $p < 0.001$ ) and left CGH ( $\beta = -0.43$ ,  $p < 0.001$ ). No

correlation was found in the groups of A-T- CN, A+T- CN, and A+T+ CN.

#### Diagnostic performance of CGH FA in preclinical AD

Table 3 shows the results of ROC analysis of FA in right and left CGH and HV to discriminate between A-T- CN, A+T- CN, and A+T+ CN groups. The discrimination between A-T- CN and A+T+ CN groups was achieved by right and left CGH FA ( $p < 0.001$ ), with the AUCs of 0.69 for right CGH FA, and 0.68 for left CGH FA. Specifically, right CGH FA achieved 74% of accuracy, 58% of sensitivity and 78% of specificity, while left CGH FA had 57% of accuracy,

Table 2  
Relationship between DTI measures and global amyloid, tau in the temporal meta-ROI, and hippocampal volume (HV)

	Amyloid-PET SUVR			Tau-PET SUVR			HV		
	$\beta$	<i>t</i>	<i>p</i>	$\beta$	<i>t</i>	<i>p</i>	$\beta$	<i>t</i>	<i>p</i>
Correlation in the Alzheimer's continuum									
right CGH FA	0.09	1.04	0.30	-0.23	-2.44	<b>0.02</b>	0.39	4.46	<b>&lt;0.001</b>
left CGH FA	0.03	0.41	0.69	-0.29	-3.18	<b>&lt;0.001</b>	0.40	4.74	<b>&lt;0.001</b>
right CGH MD	-0.07	-0.93	0.35	0.30	3.81	<b>&lt;0.001</b>	-0.44	-5.94	<b>&lt;0.001</b>
left CGH MD	-0.17	-2.27	0.03	0.36	4.24	<b>&lt;0.001</b>	-0.43	-5.35	<b>&lt;0.001</b>
Correlation in the A-T- CN group									
right CGH FA	-0.05	-0.49	0.62	0.07	0.67	0.51	0.001	0.01	0.99
left CGH FA	0.06	0.60	0.55	0.05	0.48	0.63	0.11	1.13	0.26
right CGH MD	0.07	0.65	0.52	0.10	1.03	0.30	-0.10	-0.89	0.37
left CGH MD	0.04	0.41	0.69	0.06	0.64	0.52	-0.13	-1.34	0.19
Correlation in the A+T- CN group									
right CGH FA	0.21	1.27	0.21	-0.02	-0.1	0.92	0.08	0.45	0.66
left CGH FA	0.07	0.43	0.67	-0.01	-0.05	0.96	0.24	1.33	0.19
right CGH MD	-0.06	-0.46	0.65	0.20	1.41	0.17	-0.26	-1.73	0.09
left CGH MD	-0.17	-1.11	0.28	0.15	0.97	0.34	-0.25	-1.5	0.14
Correlation in the A+T+ CN group									
right CGH FA	-0.05	-0.22	0.83	-0.18	-0.88	0.39	0.21	0.99	0.33
left CGH FA	0.04	0.20	0.84	0.05	0.25	0.81	0.43	2.06	0.05
right CGH MD	0.15	0.74	0.47	0.15	0.75	0.46	-0.06	-0.29	0.77
left CGH MD	-0.08	-0.35	0.73	-0.11	-0.49	0.63	-0.26	-1.15	0.26

Fractional anisotropy (FA) and mean diffusivity (MD) values were used as dependent variables in linear regression analysis as a function of PET SUVR values. The impact of age, sex, years of education, and WMH volume were regressed out.  $\beta$  is standardized regression coefficients. *p* values are uncorrected.

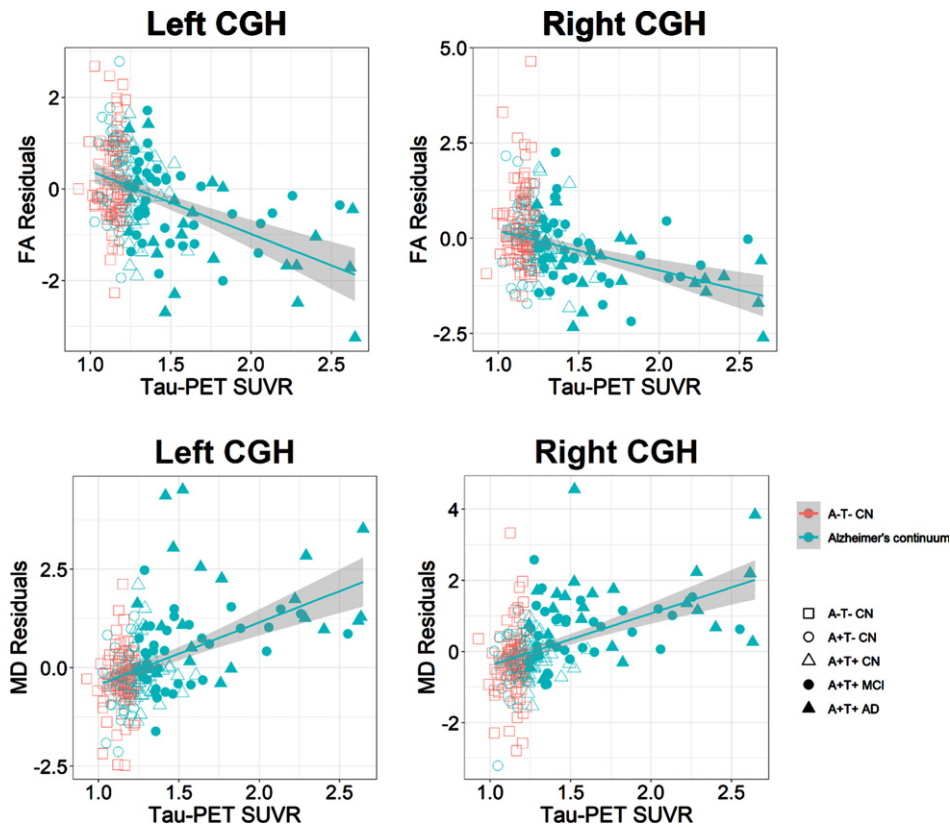


Fig. 2. Scatter plot showing the relationship between DTI measures (FA and MD) and tau-PET SUVR (temporal meta-ROI). The regression lines including the 95% CIs (shaded bands) for Alzheimer's continuum as a function of tau are displayed. The value of FA and MD are residuals after regressing out the effect of age, sex, years of education, and WMH volume.

Table 3  
Performance of DTI measures in CGH in discrimination among groups

	AUC (95%CI)	SE	<i>p</i>	Optimal Cutoff <sup>†</sup>	Accuracy (%)	Sensitivity (%)	Specificity (%)
A–T– CN versus A+T+ CN (n/n = 97/36)							
right CGH FA	0.69 (0.59–0.80)	0.003	<0.001	0.35	74	58	78
left CGH FA	0.68 (0.58–0.77)	0.003	<0.001	0.37	57	83	47
HV (cm <sup>3</sup> )	0.62 (0.51–0.72)	0.050	0.03	7.9	62	64	61
A–T– CN versus A+T– CN (n/n = 97/43)							
right CGH FA	0.61 (0.51–0.71)	0.052	0.03	0.35	67	47	76
left CGH FA	0.51 (0.40–0.61)	0.053	0.89	0.37	54	58	53
HV (cm <sup>3</sup> )	0.56 (0.46–0.67)	0.050	0.24	8.3	51	77	40
A+T– CN versus A+T+ CN (n/n = 43/36)							
right CGH FA	0.58 (0.46–0.71)	0.065	0.19	0.37	59	83	40
left CGH FA	0.68 (0.56–0.80)	0.061	<0.01	0.36	66	64	67
HV (cm <sup>3</sup> )	0.56 (0.43–0.69)	0.070	0.39	7.8	63	56	70

<sup>†</sup>Youden index-derived cutoff; AUC, area under the receiver operating characteristic curve; CI, confidence interval; SE, standard error; CN, cognitively normal; CGH, hippocampal cingulum; FA, fractional anisotropy; HV, hippocampal volume (with intracranial volume adjusted).

83% of sensitivity, and 47% of specificity. No metrics allowed the discrimination between A–T– CN and A+T– CN groups. Only left CGH FA allowed the discrimination between A+T– CN and A+T+ CN groups, with AUC of 0.68, accuracy, sensitivity, and specificity of 66%, 64%, and 67% respectively. HV did not allow discrimination between CN groups.

## DISCUSSION

This study aims to describe WM microstructural alteration on DTI in the Alzheimer's continuum defined by A $\beta$  deposition. Decreased FA and increased MD were observed across the Alzheimer's continuum, with the earliest alteration occurring in CGH at the CN stage with positive A $\beta$  and tau status. The alteration of the DTI measures in the Alzheimer's continuum was correlated with tau but not with A $\beta$ , suggesting that WM change may reflect underlying tau pathology. Furthermore, FA change in bilateral CGH allowed for the discrimination between CN subjects with and without AD pathologies. Our results encourage further investigation on diffusivity changes in the CGH region in preclinical AD.

Diffusion alteration in widespread WM tracts was observed in A+T+ MCI and A+T+ AD groups, including fornix, SLF, UF, CGC, and CGH. The findings are consistent with the previous meta-analysis in studying WM alterations in MCI, which found reliable FA and MD alterations in the above-mentioned tracts [29, 30]. Our study reinforces such alterations in WM in clinically diagnosed AD but also in biologically defined patients where A $\beta$  and tau status are considered. Such alterations occur in cumulative patterns with increasing cognitive impairment and

increasing A $\beta$  and tau load. Among the three CN groups, most tracts showed a trend of increased FA and decreased MD in the A+T– CN group, followed by a decreased FA and increased MD in the A+T+ group. However, the differences between groups did not reach a statistically significant level. A diffusion kurtosis imaging study demonstrated that subjects with intermediate A $\beta$  load displayed more restricted diffusion compared with subjects with either low or high A $\beta$  load, indicating a nonmonotonic trend in diffusion restriction in early A $\beta$  accumulation [31]. Our study further showed that the decreased diffusion restriction occurred at the stage when both A $\beta$  and tau reached a high level. Hence, a high amount of tau might account for the diffusion alteration in the later stage of A $\beta$  accumulation. A $\beta$  presence may strengthen the association between tau and WM alterations [14] and indirectly accelerate WM degradation in the long run [32].

CGH is the only tract that presented FA alteration in the CN stage between A+T+ CN and A–T– CN groups, and the FA consistently decreased in A+T+ MCI and A+T+ AD groups. Our results are in line with previous studies which found altered CGH diffusion in subjects with AD [33], MCI [33], and subjective cognitive decline [9]. CGH is the hippocampal formation part of the cingulum, thus its integrity may be partly linked to the integrity of the hippocampus. In addition, CGH is a major pathway of the limbic system, and it connects the hippocampus to the cingulate gyrus [34]. It was reported that CGH diffusivity can predict tau burden in the downstream-connected posterior cingulate cortex in A $\beta$ -positive subjects [14]. Therefore, diffusion alteration in CGH could be a potential biomarker in detecting and monitoring the early accumulation of AD pathology.

A significant correlation was observed between diffusion measures and tau but not with A $\beta$  in the Alzheimer's continuum, suggesting that tau may be a predominant factor that affects diffusion in the course of AD. Our findings on DTI correlation with tau is consistent with previous literature. The association with tau has been reported in the AD-signature region [15], and increased MD has been shown to correlate with neurofibrillary tangle at autopsy [6]. Abnormal tau hyperphosphorylation leads to decreased microtubule binding, destabilizes microtubules, and results in axonal integrity loss [15], leading to a lower FA and higher MD value. Thus, DTI measures may be a potential biomarker in monitoring the accumulation of tau pathology. As for A $\beta$ , inconsistent findings were reported on the correlation of WM alteration with A $\beta$ . Along with others [6, 15], we did not observe the correlation of diffusion measures with global A $\beta$  in the mixed cohort of cognitively unimpaired and impaired subjects, while the correlation was reported by other studies at global [35] and regional levels in terms of the cingulum, corpus callosum [13], and UF [36] in the cognitively unimpaired subjects. A $\beta$  accumulates early in the course of AD and is assumed to reach a plateau before the onset of cognitive symptoms [37], so the correlation is anticipated in the asymptomatic stage. However, we did not observe the correlation in the CN groups as well. A possible explanation for the inconsistency is that the diffusion change in CGH may correlate with A $\beta$  in the regions connected by the CGH rather than global A $\beta$  measured in this study. Further, a potential non-monotonic association [13, 35] may also not be revealed by our statistical analysis.

Right and left CGH FA allow discrimination between A-T- CN and A+T+ CN groups, and left CGH FA achieved 83% sensitivity and right CGH FA achieved 78% specificity. This finding may suggest that FA changes in the left CGH occur earlier than that in the right CGH. However, the overall diagnostic performance was not high because all the AUC values did not exceed 0.7. In addition, a wide range of AUC may not be suitable for its clinical use. Although a distinct difference in FA in CGH between subjects with and without AD pathology was detected at the CN stage, the differences may not allow for accurate discrimination at the individual level. FA in CGH has been studied for discrimination. One study used FA from all voxels within the CGH ROI to discriminate CN, MCI, and AD subjects with a support vector machine, and achieved average accuracies of 87% between AD and controls and 83% between AD

and MCI [34]. Hence, FA measurement in CGH has potential to assist in AD diagnosis.

This study has several limitations. First, as a cross-sectional study design was used, this work cannot assume that a subject with a certain level of AD pathology is temporally similar in clinical manifestation to another subject with the same level of pathology. Future longitudinal studies could better elucidate microstructural changes in CGH with increasing AD pathology over time. Second, we did not further classify subjects based on neurodegeneration due to the small sample size. Neurodegeneration may correlate more with diffusion change than A $\beta$  [10]. We controlled the neurodegeneration effect as indexed by hippocampal volume in the analysis. Further study may explore the complete spectrum of biologically defined AD with additional neurodegeneration factor added. Third, the grouping is limited to the expected progression of classic "pure" AD through the biomarker schema, of which clinical MCI or dementia do not occur until A, T, and neurodegeneration biomarkers are abnormal so the cognitive deficit is attributable to AD pathologies alone. However, other biomarker combinations do occur in the clinical MCI and dementia stage and may indicate other processes. Future study may explore the diffusion changes in MCI and dementia subjects with biomarker combinations such as A+T-. Fourth, with the ROI-based analysis adopted, the derived diffusion metrics largely rely on the accuracy of image registration. Advanced DTI analysis methods, such as tractometry, could derive fiber-specific diffusion metrics [36], which may in turn improve the diagnostic performance of diffusion metrics in CGH.

In summary, this study investigated WM alteration on DTI in the Alzheimer's continuum. Decreased FA in the hippocampal cingulum was first detected in CN subjects with high levels of A $\beta$  and tau burden and allowed for the discrimination from pathology normal subjects. Our results encourage further investigation on diffusivity changes in the CGH region in preclinical AD.

## ACKNOWLEDGMENTS

This work was supported by the Direct Grant from the Chinese University of Hong Kong (Project code: 2020.016(4054595)).

Data collection and sharing for this project was funded by the Alzheimer's Disease Neuroimaging Initiative (ADNI) (National Institutes of Health

Grant U01 AG024904) and DOD ADNI (Department of Defense award number W81XWH-12-2-0012). ADNI is funded by the National Institute on Aging, the National Institute of Biomedical Imaging and Bioengineering, and through generous contributions from the following: AbbVie, Alzheimer's Association; Alzheimer's Drug Discovery Foundation; Araclon Biotech; BioClinica, Inc.; Biogen; Bristol-Myers Squibb Company; CereSpir, Inc.; Cogstate; Eisai Inc.; Elan Pharmaceuticals, Inc.; Eli Lilly and Company; EuroImmun; F. Hoffmann-La Roche Ltd and its affiliated company Genentech, Inc.; Fujirebio; GE Healthcare; IXICO Ltd.; Janssen Alzheimer Immunotherapy Research & Development, LLC.; Johnson & Johnson Pharmaceutical Research & Development LLC.; Lumosity; Lundbeck; Merck & Co., Inc.; Meso Scale Diagnostics, LLC.; NeuroRx Research; Neurotrack Technologies; Novartis Pharmaceuticals Corporation; Pfizer Inc.; Piramal Imaging; Servier; Takeda Pharmaceutical Company; and Transition Therapeutics. The Canadian Institutes of Health Research is providing funds to support ADNI clinical sites in Canada. Private sector contributions are facilitated by the Foundation for the National Institutes of Health (<http://www.fnih.org>). The grantee organization is the Northern California Institute for Research and Education, and the study is coordinated by the Alzheimer's Therapeutic Research Institute at the University of Southern California. ADNI data are disseminated by the Laboratory for Neuro Imaging at the University of Southern California.

Authors' disclosures available online (<https://www.j-alz.com/manuscript-disclosures/22-0671r2>).

## SUPPLEMENTARY MATERIAL

The supplementary material is available in the electronic version of this article: <http://dx.doi.org/10.3233/JAD-220671>.

## REFERENCES

- [1] Vogt NM, Hunt JFV, Adluru N, Ma Y, Van Hulle CA, Iii DCD, Kecskemeti SR, Chin NA, Carlsson CM, Asthana S, Johnson SC, Kollmorgen G, Batrla R, Wild N, Buck K, Zetterberg H, Alexander AL, Blennow K, Bendlin BB (2022) Interaction of amyloid and tau on cortical microstructure in cognitively unimpaired adults. *Alzheimers Dement* **18**, 65-76.
- [2] Scheltens P, De Strooper B, Kivipelto M, Holstege H, Chételat G, Teunissen CE, Cummings J, van der Flier WM (2021) Alzheimer's disease. *Lancet* **397**, 1577-1590.
- [3] Pini L, Pievani M, Bocchetta M, Altomare D, Bosco P, Cavado E, Galluzzi S, Marizzoni M, Frisoni GB (2016) Brain atrophy in Alzheimer's disease and aging. *Ageing Res Rev* **30**, 25-48.
- [4] Sachdev PS, Zhuang L, Braidy N, Wen W (2013) Is Alzheimer's a disease of the white matter? *Curr Opin Psychiatry* **26**, 244.
- [5] Mayo CD, Mazerolle EL, Ritchie L, Fisk JD, Gawryluk JR (2017) Longitudinal changes in microstructural white matter metrics in Alzheimer's disease. *Neuroimage Clin* **13**, 330-338.
- [6] Kantarci K, Murray ME, Schwarz CG, Reid RI, Przybelski SA, Lesnick T, Zuk SM, Raman MR, Senjem ML, Gunter JL, Boeve BF, Knopman DS, Parisi JE, Petersen RC, Jack CR, Dickson DW (2017) White-matter integrity on DTI and the pathologic staging of Alzheimer's disease. *Neurobiol Aging* **56**, 172-179.
- [7] Wang S, Rao J, Yue Y, Xue C, Hu G, Qi W, Ma W, Ge H, Zhang F, Zhang X, Chen J (2021) Altered frequency-dependent brain activation and white matter integrity associated with cognition in characterizing pre-clinical Alzheimer's disease stages. *Front Hum Neurosci* **15**, 625232.
- [8] Mayo CD, Garcia-Barrera MA, Mazerolle EL, Ritchie LJ, Fisk JD, Gawryluk JR, Alzheimer's Disease Neuroimaging Initiative (2019) Relationship between DTI metrics and cognitive function in Alzheimer's disease. *Front Aging Neurosci* **10**, 436.
- [9] Shao W, Li X, Zhang J, Yang C, Tao W, Zhang S, Zhang Z, Peng D (2019) White matter integrity disruption in the pre-dementia stages of Alzheimer's disease: From subjective memory impairment to amnesic mild cognitive impairment. *Eur J Neurol* **26**, 800-807.
- [10] Kantarci K, Schwarz CG, Reid RI, Przybelski SA, Lesnick TG, Zuk SM, Senjem ML, Gunter JL, Lowe V, Machulda MM, Knopman DS, Petersen RC, Jack CR (2014) White matter integrity determined with diffusion tensor imaging in older adults without dementia: Influence of amyloid load and neurodegeneration. *JAMA Neurol* **71**, 1547-1554.
- [11] Araque Caballero MÁ, Suárez-Calvet M, Duering M, Franzmeier N, Benzinger T, Fagan AM, Bateman RJ, Jack CR, Levin J, Dichgans M, Jucker M, Karch C, Masters CL, Morris JC, Weiner M, Rossor M, Fox NC, Lee J-H, Salloway S, Danek A, Goate A, Yakushev I, Hassenstab J, Schofield PR, Haass C, Ewers M (2018) White matter diffusion alterations precede symptom onset in autosomal dominant Alzheimer's disease. *Brain* **141**, 3065-3080.
- [12] Brown EE, Rashidi-Ranjbar N, Caravaggio F, Gerretsen P, Pollock BG, Mulsant BH, Rajji TK, Fischer CE, Flint A, Mah L, Herrmann N, Bowie CR, Voineskos AN, Graff-Guerrero A; PACI-MD Study Group (2019) Brain amyloid PET tracer delivery is related to white matter integrity in patients with mild cognitive impairment. *J Neuroimaging* **29**, 721-729.
- [13] Collij LE, Ingala S, Top H, Wottschel V, Stickney KE, Tomassen J, Konijnenberg E, Ten Kate M, Sudre C, Lopes Alves I, Yaqub MM, Wink AM, Van 't Ent D, Scheltens P, van Berckel BNM, Visser PJ, Barkhof F, Braber AD (2021) White matter microstructure disruption in early stage amyloid pathology. *Alzheimers Dement (Amst)* **13**, e12124.
- [14] Jacobs HLL, Hedden T, Schultz AP, Sepulcre J, Perea RD, Amariglio RE, Papp KV, Rentz DM, Sperling RA, Johnson KA (2018) Structural tract alterations predict downstream tau accumulation in amyloid-positive older individuals. *Nat Neurosci* **21**, 424-431.

- [15] Strain JF, Smith RX, Beaumont H, Roe CM, Gordon BA, Mishra S, Adeyemo B, Christensen JJ, Su Y, Morris JC, Benzinger TLS, Ances BM (2018) Loss of white matter integrity reflects tau accumulation in Alzheimer disease defined regions. *Neurology* **91**, e313-e318.
- [16] Nelson PT, Head E, Schmitt FA, Davis PR, Neltner JH, Jicha GA, Abner EL, Smith CD, Van Eldik LJ, Kryscio RJ, Scheff SW (2011) Alzheimer's disease is not "brain aging": Neuropathological, genetic, and epidemiological human studies. *Acta Neuropathol* **121**, 571-587.
- [17] Bennett DA, Schneider JA, Arvanitakis Z, Kelly JF, Aggarwal NT, Shah RC, Wilson RS (2006) Neuropathology of older persons without cognitive impairment from two community-based studies. *Neurology* **66**, 1837-1844.
- [18] Jack CR, Jr., Bennett DA, Blennow K, Carrillo MC, Dunn B, Haeberlein SB, Holtzman DM, Jagust W, Jessen F, Karlawish J, Liu E, Molinuevo JL, Montine T, Phelps C, Rankin KP, Rowe CC, Scheltens P, Siemers E, Snyder HM, Sperling R (2018) NIA-AA Research Framework: Toward a biological definition of Alzheimer's disease. *Alzheimers Dement* **14**, 535-562.
- [19] McKhann GM, Knopman DS, Chertkow H, Hyman BT, Jack CR, Jr., Kawas CH, Klunk WE, Koroshetz WJ, Manly JJ, Mayeux R, Mohs RC, Morris JC, Rossor MN, Scheltens P, Carrillo MC, Thies B, Weintraub S, Phelps CH (2011) The diagnosis of dementia due to Alzheimer's disease: Recommendations from the National Institute on Aging-Alzheimer's Association workgroups on diagnostic guidelines for Alzheimer's disease. *Alzheimers Dement* **7**, 263-269.
- [20] Landau SM, Lu M, Joshi AD, Pontecorvo M, Mintun MA, Trojanowski JQ, Shaw LM, Jagust WJ (2013) Comparing positron emission tomography imaging and cerebrospinal fluid measurements of  $\beta$ -amyloid. *Ann Neurol* **74**, 826-836.
- [21] Jack CR, Jr., Wiste HJ, Weigand SD, Therneau TM, Lowe VJ, Knopman DS, Gunter JL, Senjem ML, Jones DT, Kantarci K, Machulda MM, Mielke MM, Roberts RO, Vemuri P, Reyes DA, Petersen RC (2017) Defining imaging biomarker cut points for brain aging and Alzheimer's disease. *Alzheimers Dement* **13**, 205-216.
- [22] Svård D, Nilsson M, Lampinen B, Lätt J, Sundgren PC, Stomrud E, Minthon L, Hansson O, van Westen D (2017) The effect of white matter hyperintensities on statistical analysis of diffusion tensor imaging in cognitively healthy elderly and prodromal Alzheimer's disease. *PLoS One* **12**, e0185239.
- [23] Leemans A, Jones DK (2009) The B-matrix must be rotated when correcting for subject motion in DTI data. *Magn Reson Med* **61**, 1336-1349.
- [24] Mori S, Oishi K, Jiang H, Jiang L, Li X, Akhter K, Hua K, Faria AV, Mahmood A, Woods R, Toga AW, Pike GB, Neto PR, Evans A, Zhang J, Huang H, Miller MI, van Zijl P, Mazziotta J (2008) Stereotaxic white matter atlas based on diffusion tensor imaging in an ICBM template. *Neuroimage* **40**, 570-582.
- [25] Jenkinson M, Bannister P, Brady M, Smith S (2002) Improved optimization for the robust and accurate linear registration and motion correction of brain images. *Neuroimage* **17**, 825-841.
- [26] Jenkinson M, Smith S (2001) A global optimisation method for robust affine registration of brain images. *Med Image Anal* **5**, 143-156.
- [27] Youden WJ (1950) Index for rating diagnostic tests. *Cancer* **3**, 32-35.
- [28] DeLong ER, DeLong DM, Clarke-Pearson DL (1988) Comparing the areas under two or more correlated receiver operating characteristic curves: A nonparametric approach. *Biometrics* **44**, 837-845.
- [29] Yu J, Lam CLM, Lee TMC (2017) White matter microstructural abnormalities in amnesic mild cognitive impairment: A meta-analysis of whole-brain and ROI-based studies. *Neurosci Biobehav Rev* **83**, 405-416.
- [30] Sexton CE, Kalu UG, Filippini N, Mackay CE, Ebmeier KP (2011) A meta-analysis of diffusion tensor imaging in mild cognitive impairment and Alzheimer's disease. *Neurobiol Aging* **32**, 2322.e2325-2322.e2318.
- [31] Dong JW, Jelescu IO, Ades-Aron B, Novikov DS, Friedman K, Babb JS, Osorio RS, Galvin JE, Shepherd TM, Fieremans E (2020) Diffusion MRI biomarkers of white matter microstructure vary nonmonotonically with increasing cerebral amyloid deposition. *Neurobiol Aging* **89**, 118-128.
- [32] Vipin A, Ng KK, Ji F, Shim HY, Lim JKW, Pasternak O, Zhou JH, Initiative AsDN (2019) Amyloid burden accelerates white matter degradation in cognitively normal elderly individuals. *Hum Brain Mapp* **40**, 2065-2075.
- [33] Zhang Y, Schuff N, Jahng G-H, Bayne W, Mori S, Schad L, Mueller S, Du A-T, Kramer JH, Yaffe K, Chui H, Jagust WJ, Miller BL, Weiner MW (2007) Diffusion tensor imaging of cingulum fibers in mild cognitive impairment and Alzheimer disease. *Neurology* **68**, 13-19.
- [34] Dalboni da Rocha JL, Bramati I, Coutinho G, Tovar Moll F, Sitaram R (2020) Fractional anisotropy changes in parahippocampal cingulum due to Alzheimer's disease. *Sci Rep* **10**, 2660.
- [35] Wolf D, Fischer FU, Scheurich A, Fellgiebel A (2015) Non-linear association between cerebral amyloid deposition and white matter microstructure in cognitively healthy older adults. *J Alzheimers Dis* **47**, 117-127.
- [36] Pichet Binette A, Theaud G, Rheault F, Roy M, Collins DL, Levin J, Mori H, Lee JH, Farlow MR, Schofield P, Chhatwal JP, Masters CL, Benzinger T, Morris J, Bateman R, Breitner JC, Poirier J, Gonneaud J, Descoteaux M, Villeneuve S, DIAN Study Group; PREVENT-AD Research Group (2021) Bundle-specific associations between white matter microstructure and A $\beta$  and tau pathology in preclinical Alzheimer's disease. *eLife* **10**, e62929.
- [37] Villemagne VL, Pike KE, Chételat G, Ellis KA, Mulligan RS, Bourgeat P, Ackermann U, Jones G, Szoeke C, Salvado O, Martins R, O'Keefe G, Mathis CA, Klunk WE, Ames D, Masters CL, Rowe CC (2011) Longitudinal assessment of A $\beta$  and cognition in aging and Alzheimer disease. *Ann Neurol* **69**, 181-192.